Dicopper(II) and Dizinc(II) Complexes with Nonsymmetric Dinucleating Ligands Based on Indolo[3,2-*c*]quinolines: Synthesis, Structure, Cytotoxicity and Intracellular Distribution

Michael F. Primik,[#] Simone Göschl,[#] Samuel M. Meier,[#] Nadine Eberherr,[#] Michael A. Jakupec,[#] Éva A. Enyedy,[‡,†] Ghenadie Novitchi,[§] Vladimir B. Arion*[,#]

[#]Institute of Inorganic Chemistry, University of Vienna, Währinger Str. 42, A-1090 Vienna, Austria

[‡]Department of Inorganic and Analytical Chemistry, University of Szeged, Dóm tér 7, H-6720, Szeged, Hungary

[†]HAS-USZ Bioinorganic Chemistry Research Group, Dóm tér 7, H-6720 Szeged, Hungary

[§]Laboratoire National des Champs Magnétiques Intenses-CNRS, 25 Avenue des Martyrs, 38042 Grenoble Cedex 9, France

Abstract: Dicopper(II) and dizinc(II) complexes $[Cu_2(^{MeOOC}L^{COO})(CH_3COO)_2]\cdot 3CH_3OH$ (**1**) and $[Zn_2(^{MeOOC}L^{COO})(CH_3COO)_2]\cdot 2CH_3OH$ (**2**) were synthesized by reaction of $Cu(CH_3COO)_2\cdot H_2O$ and $Zn(CH_3COO)_2\cdot 2H_2O$ with a new nonsymmetric dinucleating ligand ^{EtOOC}**HL**^{COOEt} prepared by condensation of 6-hydrazinyl-11*H*-indolo[3,2-*c*]quinoline with diethyl-2,2′-((3-formyl-2-hydroxy-5-methylbenzyl)azanediyl)diacetate. The design and synthesis of this elaborate ligand was performed with the aim of increasing the aqueous solubility of indolo[3,3-*c*]quinolines, known as biologically active compounds, and investigating the antiproliferative activity in human cancer cell lines and the cellular distribution by exploring the intrinsic fruorescence of indoloquinoline scaffold. The compounds have been comprehensively characterized by elemental analysis, spectroscopic methods (IR, UV–vis, ^{1}H and ^{13}C NMR spectroscopy), ESI mass spectrometry, magnetic susceptibility measurements and UV–vis complex formation studies (for **1**), as well as by X-ray crystallography (**1** and **2**). The antiproliferative activity of ^{EtOOC}**HL**^{COOEt}, **1** and **2** was determined by MTT assay in three human cancer cell lines, namely, A549 (nonsmall cell lung carcinoma, CH1 (ovarian carcinoma) and SW480 (colon adenocarcinoma) yielding IC_{50} values in the micromolar concentration range and showing dependence on the cell line used. The effect of metal coordination on cytotoxicity of ^{EtOOC}**HL**^{COOEt} is also discussed. Subcellular distribution of ^{EtOOC}**HL**^{COOEt} and **2** was investigated by fluorescence microscopy in human cancer cell lines and revealed similar localization for both compounds in cytoplasmic structures.

Keywords: nonsymmetrical hybrid ligands, indolo[3,2-*c*]quinolines, copper(II), zinc(II), antiproliferative activity

Introduction

Cancer is a disease difficult to treat and novel drugs are still highly demanded.[1–3] Metal complexes with biologically active ligands have become increasingly important in the development of anticancer drugs, as metal ions can significantly alter their physical and biological properties.[4–7] Indolo[3,2-*d*]benzazepines, also referred to as paullones, represent a class of potential cyclin-dependent kinase (Cdk) inhibitors, identified in a comparative database search at the National Cancer Institute (NCI; NCI60 screen), where the lead compound kenpaullone exhibited an activity profile similar to that of flavopiridol,[8,9] the first clinically tested Cdk inhibitor. Notably, the antiproliferative activity of kenpaullone does not parallel its Cdk inhibitory profile. As a result other intracellular targets for this class of compounds, e.g. glycogen synthase kinase 3β (Gsk3β) or mitochondrial malate dehydrogenase (mMDH), have been suggested.[10] Despite the directed efforts on their development as anticancer drugs, paullones remain at an early preclinical stage mainly because of their low aqueous solubility and bioavailability. Metal coordination was suggested as a means to overcome these problems. As original paullones did not contain binding sites for metal ions, these were created by chemical modification of their molecular structure. A library of paullone-based ligands with a broad structural diversity and complexes with copper(II), gallium(III), ruthenium(II) and osmium(II) have been reported.[11–15]

In an effort to elucidate novel structure–activity relationships (SARs) the folded seven-membered azepine ring of paullones has been replaced by a pyridine ring leading to another class of biologically active compounds, namely indolo[3,2-*c*]quinolines, with an essentially planar structure. Indolo[3,2-*c*]quinolines and the structurally related

indolo[3,2-*b*]quinolines have been isolated from the roots of the West African climbing shrub *Cryptolepsis sanguinolenta*, used in traditional African medicine. Both exhibit a broad spectrum of biological properties, including antibacterial, antitumor, as well as anti-inflammatory activity.[16] In contrast to indolo[3,2-*b*]quinolines, only few studies have been conducted for indolo[3,2-*c*]quinolines so far. Like paullones, indoloquinolines do not contain binding sites for metal ions. However, these can be introduced by exploring chemistry tools essentially different from those applied for paullones. The first ruthenium(II), osmium(II) and copper(II) complexes with indolo[3,2-*c*]quinoline modified ligands were derived from structurally related paullone complexes, by using distinct chemical transformations, and studies aimed at the discovery of novel SARs have been performed.[17–20] In particular, it has been found that indolo[3,2-*c*]quinolines exhibit higher cytotoxicity compared to their paullone-counterparts. In other words the effect of replacement of seven-membered azepine ring in paullones by a pyridine ring in indoloquinolines has been clearly established. In addition, it was shown that SARs of paullone-modified complexes do not necessarily apply to indolo[3,2-*c*]quinoline-based compounds.[17,19] Current efforts by us are focused on the investigation of the underlying mechanisms of their antiproliferative activity. In this regard, the intrinsic fluorescence of indolo[3,2-*c*]quinolines can also be explored.[21]

Recently we published the syntheses of highly antiproliferative copper(II) complexes with modified indolo[3,2-*c*]quinolines.[19] Herein we report on the synthesis of a more elaborate bioligand with two distinct binding sites, and its dinuclear copper(II) and zinc(II) complexes. The new bioconjugate is sufficiently soluble in various biological media and intrinsically fluorescent when light-irradiated at λ_{ex} = 395 nm. These

properties permitted us to track the intracellular distribution of the ligand and its zinc(II) complex. Moreover, the ligand design led to assembly of homometallic dinuclear complexes with distinct compartments (Scheme 1), a feature not explored by us so far in the development of anticancer metal complexes.

Scheme 1. Synthesis of $^{EtOOC}HL^{COOEt}$, **1** and **2**[a] and atom numbering schemes for modified indoloquinolines.

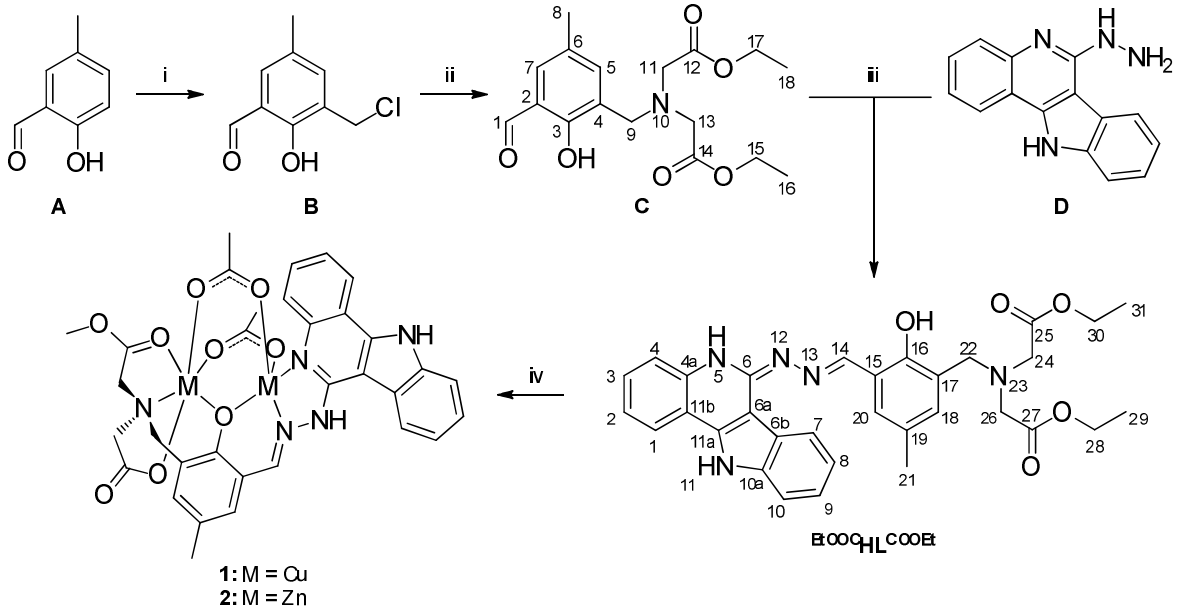

[a] Reagents and conditions: (i) 35% formaldehyde solution, conc. HCl;[22,23] (ii) diethyl-2,2'-iminodiacetate, triethylamine, dry THF, room temperature, 3 h (95%); (iii) methanol, room temperature, 2 h (95%); (iv) copper(II) acetate monohydrate or zinc(II) acetate dihydrate, methanol, room temperature, 30 min [**1** (37%), **2** (33%)].

Experimental Section

Materials. All chemicals were purchased from commercial suppliers and were used without further purification. Hydrochloric acid, 4-(2-hydroxyethyl)-1-piperazineethanesulfonic acid (HEPES), 2-hydroxy-5-methylbenzaldehyde (**A**), diethyl-

2,2'-iminodiacetate and guanosine 5'-triphosphate were received from Sigma-Alrdich. L-histidine, formaldehyde solution (35%), copper(II) acetate monohydrate and zinc acetate dihydrate from Merck and tetrahydrofuran (THF) and methanol (both analytical reagent grade) from Fisher Scientific. THF was dried prior to use by a standard protocol. Dimethyl sulfoxide (DMSO) was received from Acros, ammonium bicarbonate, formic acid and L-glutamic acid from Fluka and L-aspartic acid from Serva. MilliQ water (18.2 MΩ, Millipore Advantage A10, 185 UV Ultrapure Water System, Molsheim, France) and methanol (Fisher, HPLC grade) were used for ESI-MS experiments. 6-Hydrazinyl-11*H*-indolo[3,2-*c*]quinolone (**D**, Scheme 1) was synthesized according to the published protocol.[18] 3-(chloromethyl)-2-hydroxy-5-methylbenzaldehyde (**B**) was obtained from 5-methyl-2-hydroxybenzaldehyde (**A**) via a previously described chloromethylation reaction.[22,23]

Diethyl-2,2'-((3-formyl-2-hydroxy-5-methylbenzyl)azanediyl)diacetate (C). To a stirred solution of 3-(chloromethyl)-2-hydroxy-5-methylbenzaldehyde (0.100 g, 0.54 mmol) in dry THF (30 mL) was added diethyl-2,2'-iminodiacetate (85 μL, 0.48 mmol) under argon atmosphere. Upon addition of triethylamine (281 μL, 2.0 mmol) the colorless solution turned brightly yellow and a white precipitate formed. After stirring for 3 h at room temperature, the precipitate was filtered off. The yellow filtrate was concentrated under reduced pressure to give an orange oil which was dried *in vacuo* overnight. Yield: 0.17 g (95%), ^{1}H NMR 500.13 MHz (DMSO-d_6, δ_H, ppm): 10.60 (s, 1H, OH), 10.23 (s, 1H, C1), 7.43 (d, 1H, $^{4}J(H_{C5})$ = 2.0 Hz, C7), 7.32 (d, 1H, $^{4}J(H_{C7})$ = 2.1 Hz, C5), 4.12 (q, 4H, $^{3}J(H_{C16,\ C18})$ = 7.1 Hz, C15, C17), 3.90 (s, 2H, C9), 3.54 (s, 4H, C11, C13), 2.26 (s, 3H, C8), 1.20 (t, 6H, $^{3}J(H_{C15,\ C17})$ = 7.1 Hz, C16, C18). $^{13}C\{^{1}H\}$ NMR

125.76 MHz (DMSO-d_6, δ_C, ppm): 192.9 (C1), 171.2 (C12, C14), 158.3 (C3), 137.9 (C5), 129.1 (C7), 128.6 (C6), 125.2 (C4), 122.3 (C2), 60.8 (C15, C17), 54.4 (C11, C13), 53.6 (C9), 20.3 (C8), 14.5 (C16, C18).

Diethyl-2,2'-((3-(((5*H*-indolo[3,2-*c*]quinolin-6(11*H*)-ylidene)hydrazono)methyl)-2-hydroxy-5-methylbenzyl)azanediyl)diacetate (^{EtOOC}HL^{COOEt}). To a solution of **C** (776 mg, 2.3 mmol) in methanol (40 mL) was added **D** (544 mg, 2.2 mmol) The reaction mixture turned into a brightly yellow suspension, which was stirred for 2 h under argon atmosphere and allowed to stand at 4 °C overnight. The yellow product was filtered off, washed with cold methanol (2 × 4 mL) and dried *in vacuo* overnight. Yield: 0.77 g, 95%. Anal. Calcd for $C_{32}H_{33}N_5O_5 \cdot H_2O$ (M_r = 585.65): C, 65.63; H, 6.02; N, 11.96. Found: C, 65.75; H, 5.85; N, 11.51. ^{1}H NMR 500.13 MHz (DMSO-d_6, δ_H, ppm): 12.46 (s, 1H, N11), 10.72 (s, 1H, N5), 10.63 (s, 1H, OH), 8.77 (s, 1H, C14), 8.43 (d, 1H, $^3J(H_{C8})$ = 7.8 Hz, C7), 8.11 (d, 1H, $^3J(H_{C2})$ = 7.8 Hz, C1), 7.80 (d, 1H, $^3J(H_{C3})$ = 8.3 Hz, C4), 7.61 (d, 1H, $^3J(H_{C9})$ = 8.3 Hz, C10), 7.59 (s, 1H, C20), 7.50 – 7.44 (m, 1H, C3), 7.40 – 7.35 (m, 1H, C9), 7.30 – 7.22 (m, 2H, C8, C2), 7.10 (s, 1H, C18), 4.13 (q, 4H, $^3J(H_{C29, C31})$ = 7.1 Hz, C28, C30), 3.94 (s, 2H, C22), 3.57 (s, 4H, C24, C26), 2.30 (s, 3H, C21), 1.21 (t, 6H, $^3J(H_{C28, C30})$ = 7.1 Hz, C29, C31). ^{13}C{^{1}H} NMR 125.76 MHz (DMSO-d_6, δ_C, ppm): 171.2 (C25, C27), 154.0 (C16), 152.1 (C14), 150.1 (C6), 138.6 (C10a), 138.5 (C11a), 138.3 (C4a), 132.1 (C18), 129.5 (C3), 129.2 (C20), 127.8 (C19), 124.3 (C9), 124.2 (C17), 124.1 (C6b), 122.9 (C7), 122.2 (C1), 121.9 (C2), 121.2 (C8), 120.8 (C15), 117.1 (C4), 113.6 (C11b), 112.0 (C10), 105.2 (C6a), 60.6 (C28, C30), 54.5 (C24, C26), 53.1 (C22), 20.7 (C21), 14.6 (C29, C31). ESI-MS (methanol), positive: *m/z* 379 [HL-$C_8H_{14}NO_4$]$^+$, 568 [^{EtOOC}**HL**^{COOEt} + H^+]$^+$, 590 [^{EtOOC}**HL**^{COOEt} + Na^+]$^+$; negative: *m/z* 566

[^{EtOOC}**HL**^{COOEt} – H^+]$^-$, 603 [^{EtOOC}**HL**^{COOEt} + Cl^-]$^-$. UV–vis (methanol), λ_{max} (ε, M^{-1} cm^{-1}): 226 (43300), 260 (32350), 273 sh (25300), 306 (22400), 348 (15250), 365 sh (15900), 382 (17300). ATR-IR, selected bands, cm^{-1}: 3640, 3375, 2976, 1730, 1608, 1461, 1192, 1002.

Di(μ-acetato-κ^2*O*,*O*′)-(2-((3-((2-(11*H*-indolo[3,2-*c*]quinolin-6-yl-κ*N*^{5})hydrazono-κ*N*^{13})methyl)-5-methyl-2-oxidobenzyl-κ*O*^{1})(2-methoxy-2-oxoethyl-κ*O*^{5})amino κ*N*^{23})acetato-κ*O*^{2})-dicopper(II) (1). To a suspension of ^{EtOOC}**HL**^{COOEt} (0.200 g, 0.35 mmol) in methanol (15 mL) was added copper(II) acetate monohydrate (0.157 g, 0.78 mmol). After stirring for 30 min the dark-green solution was allowed to stand at 25 °C to evaporate slowly. After three days, X-ray diffraction quality green crystals formed were filtered off, dried *in vacuo* overnight, and stored under argon atmosphere. Yield: 0.105 g, 37%. Anal. Calcd for $C_{33}H_{31}Cu_2N_5O_9 \cdot 1.5H_2O$ (M_r = 795.72): C, 49.81; H, 4.31; N, 8.80. Found: C, 49.57; H, 4.30; N, 8.64. ESI-MS (methanol), positive: *m/z* 604 unidentified, 648 [**1** – (HOAc) – (OAc)]$^+$, 680 [**1** – $(OAc)_2$ + (CH_3O)]$^+$. UV–vis (methanol), λ_{max} (ε, M^{-1} cm^{-1}): 235 (60800), 272 (41000), 296 (24540), 354 (18900), 420 sh (20800), 441 (22700). ATR-IR, selected bands, cm^{-1}: 1737, 1583, 1540, 1385, 1217, 1028.

Di(μ-acetato-κ^2*O*,*O*′)-(2-((3-((2-(11*H*-indolo[3,2-*c*]quinolin-6-yl-κ*N*^{5})hydrazono-κ*N*^{13})methyl)-5-methyl-2-oxidobenzyl-κ*O*^{1})(2-methoxy-2-oxoethyl-κ*O*^{5})amino κ*N*^{23})acetato-κ*O*^{2})-dizinc(II) (2). To a suspension of ^{EtOOC}**HL**^{COOEt} (0.140 g, 0.25 mmol) in methanol (15 mL) was added zinc acetate dihydrate (0.124 g, 0.57 mmol). After stirring for 30 min the yellow solution was allowed to stand at 25 °C to evaporate slowly. After four days cold pentane was added and the mixture allowed to stand at 4 °C for 3 h.

The yellow precipitate formed was filtered off, dried *in vacuo* overnight and stored under argon atmosphere. Yield: 0.065 g (33%). Anal. Calcd for $C_{33}H_{31}N_5O_9Zn_2 \cdot CH_3OH \cdot H_2O$ (M_r = 822.46): C, 49.65; H, 4.53; N, 8.52. Found: C, 49.96; H, 4.35; N, 8.25. ^{1}H NMR 500.13 MHz (DMSO-d_6, δ_H, ppm): 12.33-11.60 (bs, 2H, N11, N12), 8.62-6.71 (bm, 11H, C1-4, 7-10, 14, 18, 20), 4.00-3.53 (bm, 9H, C22, 24, 26, 28), 2.22 (s, 3H, C21), 1.88 (bs, 6H, CH_3COO). ESI-MS (methanol), positive: *m/z* 668 [**2** – $(OAc)_2$ – (CH_3) + (CH_3OH)]$^+$, 682 [**2**– $(OAc)_2$ + (CH_3O)]$^+$, 710 [**2** – (OAc)]$^+$, 724 unidentified, 784 unidentified. UV–vis (methanol), λ_{max} (ε, M^{-1} cm^{-1}): 230 (44400), 258 (45700), 290 (27900), 309 (31000), 330 (17900), 346 (18200), 394 (18900). ATR-IR, selected bands, cm^{-1}: 1744, 1706, 1583, 1407, 1216, 1012. X–ray diffraction quality crystals were picked from the reaction vessel prior to addition of pentane.

Physical Measurements and Instrumentation. ^{1}H, ^{13}C and two-dimensional ^{1}H-^{1}H COSY, ^{1}H-^{1}H TOCSY, ^{1}H-^{13}C HSQC and ^{1}H-^{13}C HMBC NMR spectra were recorded on a Bruker Avance III spectrometer (Ultrashield Magnet) in DMSO-d_6 at 25 °C using standard pulse programs at 500.13 (^{1}H) and 125.76 (^{13}C) MHz. ^{1}H and ^{13}C NMR chemical shifts are quoted relative to the residual solvent signals. Elemental analyses were carried out at the Microanalytical Service of the Faculty of Chemistry of the University of Vienna. Electrospray ionization mass spectrometry was performed on a Bruker Esquire 3000 instrument (Bruker Daltonic, Bremen, Germany) on samples dissolved in methanol. UV–vis spectra were recorded with an Agilent 8453 spectrophotometer in the 190 to 1000 nm window, using samples dissolved in methanol at 10 μM concentrations. IR spectra were measured with a Bruker Vertex 70 Fourier transform IR spectrometer by means of the attenuated total reflection (ATR) technique.

Fluorescence excitation and emission spectra were recorded with a Horiba FloroMax-4 spectrofluorimeter and processed using the FluorEssence v3.5 software package. Samples of $^{EtOOC}\mathbf{HL}^{COOEt}$ and **2** were prepared from a 1 mM solution of each in DMSO and dilution with HEPES buffer (20 mM, pH = 7.4) to give samples at 10 μM concentrations with a maximum content of 1% DMSO (v/v).

Crystallographic Structure Determination. X-ray diffraction measurements were performed on a Bruker X8 APEXII CCD diffractometer. Single crystals were positioned at 40 mm from the detector, and 1312 and 722 frames were measured, each for 60 and 90 s over 1° scan width for **1**·3CH_3OH and **2**·2CH_3OH, correspondingly. The data were processed using SAINT software.[24] Crystal data, data collection parameters, and structure refinement details are given in Table 1. The structures were solved by direct methods and refined by full-matrix least-squares techniques. Non-H atoms were refined with anisotropic displacement parameters, while H atoms were inserted in calculated positions and refined with a riding model. The following software programs were used: structure solution, *SHELXS-97*; refinement, *SHELXL-97*; [25] molecular diagrams, *ORTEP*; [26] computer, Intel CoreDuo.

Table 1. Crystal data and details of data collection for **1**·3CH_3OH and **2**·2CH_3OH.

	1·3CH_3OH	**2**·2CH_3OH
empirical formula	$C_{36}H_{43}Cu_2N_5O_{12}$	$C_{35}H_{39}N_5O_{11}OZn_2$
fw	864.83	836.45
space group	*P*–1	*P*–1
a [Å]	11.1929(5)	10.7024(5)
b [Å]	11.3582(5)	11.6277(5)
c [Å]	15.4454(7)	15.4646(8)
α [°]	71.745(2)	99.404(3)
β [°]	76.682(3)	105.532(3)
γ [°]	81.086(2)	94.840(3)
V [Å^3]	1807.32(14)	1812.59(15)

Z	2	2
λ [Å]	0.71073	0.71073
ρ_{calcd} [g cm^{-3}]	1.589	1.533
crystal size [mm^3]	0.20 × 0.10 × 0.02	0.15 × 0.15 × 0.10
T [K]	120(2)	120(2)
μ [mm^{-1}]	1.249	1.533
R_1[a]	0.0418	0.0485
wR_2[b]	0.1242	0.1420
GOF[c]	1.071	1.084

[a] $R_1 = \Sigma||F_o| - |F_c||/\Sigma|F_o|$. [b] $wR_2 = \{\Sigma[w(F_o^2 - F_c^2)^2]/\Sigma[w(F_o^2)^2]\}^{1/2}$. [c] GOF = $\{\Sigma[w(F_o^2 - F_c^2)^2]/(n - p)\}^{1/2}$, where n is the number of reflections and p is the total number of parameters refined.

Magnetic Studies. Magnetic measurements were carried out on a microcrystalline sample of **1** with a Quantum Design SQUID magnetometer (MPMS-XL). Variable-temperature (2–300 K) direct current (dc) magnetic susceptibility was measured under an applied magnetic field of 0.1 T. All data were corrected for the contribution of the sample holder and diamagnetism of the samples estimated from Pascal's constants.[27,28] The analysis of the magnetic data was carried out by fitting the $\chi_M T(T)$ and $\chi_M(T)$ thermal variations including temperature independent paramagnetism (*TIP*), impurity contribution (ρ), and intermolecular interaction (zJ')[28,29,30] according to the expression:

$$\chi_M(T) = \frac{\chi_d(T)}{\left[1 - \frac{2zJ'\chi_d(T)}{Ng^2\beta^2}\right]}(1-\rho) + \rho\frac{Ng^2\beta^2}{3kT}S(S+1) + TIP$$

UV–vis Titration Studies. Complex formation was studied by UV–vis titration of 10 and 250 μM solutions of ^{EtOOC}**HL**^{COOEt} in methanol with 10 μL aliquotes of 0.5 mM and 6.25 mM stock solutions of copper(II) acetate monohydrate, respectively. One aliquote was added at 2 min intervals followed by the homogenization of the solutions as within this period the equilibrium could be reached. An Agilent 8453 spectrophotometer was used to record the UV–vis spectra in the 190 to 1000 nm window. The path length was 1 cm.

Stability constants and the molar absorbance spectra of the individual copper(II) complexes were calculated by the computer program PSEQUAD.[31]

ESI–MS Studies. Electrospray ionization mass spectra were recorded on an AmaZon SL ion trap mass spectrometer (Bruker Daltonics GmbH, Bremen, Germany). Experimental data was acquired using Compass 1.3 software and processed using Data Analysis 4.0 (Bruker Daltonics GmbH, Bremen, Germany). The experimentally obtained mass signals include a standard deviation of $m/z \pm 0.06$. The general instrument parameters were set as follows: Positive ion mode (HV –4.5 kV, RF level 89%, trap drive 74.4, dry temperature 250 °C, nebulizer 8 psi, dry gas 6 L/min and average accumulation time 144 μs), negative ion mode (HV 4.5 kV, RF level 89%, trap drive 63.8, dry temperature 250 °C, nebulizer 8 psi, dry gas 6 L/min and average accumulation time 2 ms). The samples were diluted with water : methanol (50 : 50) or water : methanol : formic acid (50 : 50 : 0.2) to a final metal concentration of 5–10 μM and measured by direct infusion into the mass spectrometer at a flow rate of 4 μL/min. Stock solutions of **1** and **2** in DMSO (10 mM) were prepared and stored at –20 °C in the dark. Each compound was diluted in ammonium carbonate buffer (20 mM, pH = 6) to give a solution of 100 μM of each compound (with 1% DMSO content). Furthermore, a solution containing L-histidine (His), L-aspartic acid (Asp), L-glutamic acid (Glu) and guanosine 5'-triphosphate (GTP) in equimolar amounts (100 μM each) and a solution containing His, Asp, Glu, GTP (each 100 μM) and ascorbic acid (Asc, 400 μM) were prepared in the same buffer. The metal-containing solutions were diluted with buffer or mixed with the solutions containing the amino acids and Asc at equimolar ratios to give a final metal concentration in each incubation mixture of 50 μM. The reaction mixtures were incubated at 37 °C and aliquots

were measured directly after mixing and after 1, 3, 5 and 24 h. Detection of **1** and **2** in electrospray ionization mass spectrometry (ESI MS) experiments required dilution with water : methanol (1 : 1) and incubation in ammonium carbonate (20 mM, pH = 7.95). The slightly acidic ammonium acetate buffer (20 mM, pH = 6) was avoided, because it lead to partial metal release. Dilution with water resulted in a low ionization in the positive and negative ion modes.

Cell Lines and Cell Culture Conditions. For cytotoxicity determination, three different human cancer cell lines were used: A549 (non-small cell lung cancer) and SW480 (colon carcinoma) (both kindly provided by Brigitte Marian, Institute of Cancer Research, Department of Medicine I, Medical University Vienna, Austria) as well as CH1 (ovarian carcinoma) (kindly provided by Lloyd R. Kelland, CRC Centre for Cancer Therapeutics, Institute of Cancer Research, Sutton, U.K.). Cells were grown as adherent monolayer cultures in 75 cm^2 culture flasks (StarLab, CytoOne) in Minimal Essential Medium supplemented with 10% heat-inactivated fetal bovine serum, 1 mM sodium pyruvate, 1% v/v non-essential amino acids (from 100× ready-to-use stock) and 4 mM L-glutamine but without antibiotics at 37 °C under a moist atmosphere containing 5% CO_2 and 95% air. All cell culture media and reagents were purchased from Sigma-Aldrich Austria.

Cytotoxicity Assay. Cytotoxicity was determined by the colorimetric MTT assay (MTT = 3-(4,5-dimethyl-2-thiazolyl)-2,5-diphenyl-2*H*-tetrazolium bromide) as described previously.[19] Briefly, cells were harvested by trypsinisation and seeded in medium (*vide supra*) into 96-well plates in volumes of 100 µL/well. Depending on the cell line,

different cell densities were used to ensure exponential growth of the untreated controls during the experiment: 1.0×10^3 (CH1), 2.0×10^3 (SW480), 3.0×10^3 (A549) cells per well. In the first 24 h the cells were allowed to settle and resume exponential growth. Then the test compounds were dissolved in DMSO, serially diluted in medium and added to the plates in volumes of 100 µL/well so that the DMSO content did not exceed 1%. Due to limited solubility of ^{EtOOC}**HL**^{COOEt} and **1**, the medium in the wells used for the highest concentrations was replaced with 200 µL/well of medium containing the test compounds. After continuous exposure for 96 h (in the incubator at 37 °C and under 5% CO_2), the medium was replaced with 100 µL/well RPMI 1640 medium (supplemented with 10% heat-inactivated fetal bovine serum and 4 mM *L*-glutamine) and MTT solution (MTT reagent in phosphate-buffered saline, 5 mg/mL) in a ratio of 7:1, and plates were incubated for further 4 h. Then the medium/MTT mixture was removed and the formed formazan was dissolved in DMSO (150 µL/well). Optical densities at 550 nm were measured (reference wavelength: 690 nm) with a microplate reader (ELX880, BioTek). The quantity of viable cells was expressed as a percentage of untreated controls, and 50% inhibitory concentrations (IC_{50}) were calculated from the concentration-effect curves by interpolation. Every test was repeated in at least three independent experiments, each consisting of three replicates per concentration level.

Fluorescence microscopy. SW480, A549 and CH1 cells were seeded in medium on cover slips in 6-well plates and allowed to settle and resume exponential growth for 24 h. Then cell were incubated for 1–2 h with 5 µM of **2** or 10 µM of ^{EtOOC}**HL**^{COOEt}, in medium. Co-staining with ER-Tracker Red and Lyso-Tracker Red (Invitrogen) was

performed according to the manufacturer's instructions. After staining, each slide was washed three times in PBS. A fluorescence microscope BX40 (Olympus) with F-View CCD Camera (Olympus), Cell^F fluorescence imaging software (Olympus) and 60× magnification oil immersions objective lens were used.

Results and Discussion

Synthesis and Characterization. The syntheses of the ligand ^{EtOOC}**HL**^{COOEt} and copper(II) and zinc(II) complexes **1** and **2**, respectively, were carried out as shown in Scheme 1. We prepared a potentially hexadentate nonsymmetric ligand consisting of two chelating arms, one able to provide a facial coordination to an octahedral metal ion, while the second exhibits a meridional binding mode. Ester functionalities are frequently introduced into the structure of organic molecules to improve their aqueous solubility and bioavailability.[32]

Recently, our group reported on the conjugation of L- and/or D-proline to 3-(chloromethyl)-2-hydroxy-5-methylbenzaldehyde (**B**), after chloromethylation of 2-hydroxy-5-methylbenzaldehyde (**A**) (Scheme 1). [33] Similarly, we reacted 3-(chloromethyl)-2-hydroxy-5-methylbenzaldehyde (**B**) with diethyl-2,2'-iminodiacetate and triethylamine in dry THF at room temperature yielding diethyl-2,2'-((3-formyl-2-hydroxy-5-methylbenzyl)azanediyl)-diacetate (**C**) as an orange oil in excellent yield (95%). The ligand ^{EtOOC}**HL**^{COOEt} was obtained by reacting **C** with 6-hydrazinyl-11*H*-indolo[3,2-*c*]quinoline (**D**)[18] in methanol at room temperature, again in excellent yield (95%). Complexes **1** and **2** were synthesized in 37 and 33% yields starting from the

ligand $^{EtOOC}\mathbf{HL}^{COOEt}$ and copper(II) acetate monohydrate, and/or zinc(II) acetate dihydrate, respectively, in methanol at room temperature. Complexation reaction in both cases is accompanied by hydrolysis of one ethyl ester group and transesterification of another ethyl ester function with formation of a new ligand $^{MeOOC}\mathbf{HL}^{COOH}$. Both generated donor arms are involved in coordination to copper(II) and zinc(II) in **1** and **2**, respectively, via the deprotonated carboxylate group and the carbonyl oxygen of the methyl ester group (see Scheme 1, Figures 1 and 2).

The new ligand $^{EtOOC}\mathbf{HL}^{COOEt}$ and its zinc(II) complex **2** have been characterized by one- and two-dimensional NMR spectroscopy, ESI mass spectrometry, elemental analysis, UV–vis and ATR-IR spectroscopy, while copper(II) complex **1** by magnetic susceptibility measurements, ESI mass spectrometry and optical spectroscopy. Additionally, both complexes have been characterized by X-ray crystallography.

The ^{1}H and ^{13}C NMR spectral data of intermediate **C**, ligand $^{EtOOC}\mathbf{HL}^{COOEt}$ and zinc(II) complex **2** along with their assignments are given in the Experimental Section. The presence of a proton at N^5 in the ^{1}H NMR spectra and the chemical shift of neighboring C^6 in the ^{13}C NMR spectra indicate that the ligand adopts a configuration with an exocyclic $C^6{=}N^{12}$ double bond. ESI mass spectra of **1** and **2** in methanol showed peaks that confirmed the formation of dimetal complexes. The most abundant peaks at *m/z* 680 and 682 for **1** and **2**, correspondingly, were assigned to $[\mathbf{1}/\mathbf{2} - (OAc)_2 + (CH_3O)]^+$.

The UV–vis spectra of $^{EtOOC}\mathbf{HL}^{COOEt}$ and **1** and **2** in methanol are depicted in Figure S1 (Supporting Information). Metal coordination led to pronounced changes in the visible range of the ligand spectrum, namely to an evolution of an absorption band at ca. 400 nm for **2** and the formation of a broad charge–transfer band at 440 nm for **1**.

X-ray crystallography. The results of X-ray diffraction studies of **1**·3CH_3OH and **2**·2CH_3OH shown in Figures 1 and 2, respectively confirm the formation of dinuclear complexes with the two copper(II) ions and zinc(II) ions bridged by the phenolate oxygen and two exogenous μ_2-η^1:η^1 acetato ligands.[34] Both copper(II) ions in **1** are distorted square-pyramidal, with τ = 0.27[35] for Cu1 with the bridging phenolate oxygen O1 in apical position, and tertiary amine N23, atoms O6 and O8 of the two bridging acetates and one aminoacetate O2 in the basal plane. We do not describe the coordination environment around Cu1 as octahedral, since the interaction between Cu1 and O5 of the dangling methyl ester group is extremely weak (Cu1···O5 2.946(2) Å). For Cu2 a distorted square-pyramidal coordination geometry (τ = 0.22) was realized with a bridging phenolate oxygen O1, quinoline nitrogen N5, hydrazinic nitrogen N13 and one oxygen atom O9 of bridging acetate in a basal plane, and another bridging acetate oxygen atom O7 in apical position.

Unlike **1**, the coordination environments of zinc(II) ions in **2** differ from each other. Zn1 has an octahedral environment built up by the bridging phenolate oxygen O1, tertiary amine donor N23, methyl ester oxygen O5 and atom O6 of the bridging acetate in equatorial positions and two oxygen atoms, one aminoacetate O2 and second O8 of abridging acetate in apical positions. Zn2 in contrast to Cu2 shows a more pronounced tendency towards a trigonal-bypyramidal coordination geometry (τ = 0.47) of the same donor atoms. Cu2 lies in the mean plane through Cu2N5C6N12N13 in **1**, while Cu1 comes out from this plane by 1.307 Å. In **2** the deviation of Zn1 from the mean plane through Zn2N5C6N12N13 is markedly smaller (0.820 Å), while distortion from planarity of the indoloquinoline moiety is more evident than in **1**. The bridging of copper(II) ions

via phenolate oxygen results in distinct Cu1–O1 and Cu2–O1 bond distances. The difference between them (0.39 Å) is larger than in other nonsymmetrically μ-phenoxido bridged dicopper(II) complexes, in which the two copper(II) ions in addition are bridged by at least one exogenous μ_2-η^1:η^1 acetato group.[36,37] The Cu1–O6 bond distance is markedly shorter than Cu2–O7, and Cu1–O8 is also shorter than Cu2–O9 (see caption to Figure 1). The Cu1···Cu2 distance in the complex is at 3.2897(6) Å, which is comparable with Cu···Cu distances of 3.297(3) Å[38] and 3.263(2) Å[39] in dicopper(II) complexes with symmetric dinucleating ligands, containing a di-μ-acetato-μ-phenolato-dicopper(II) core.

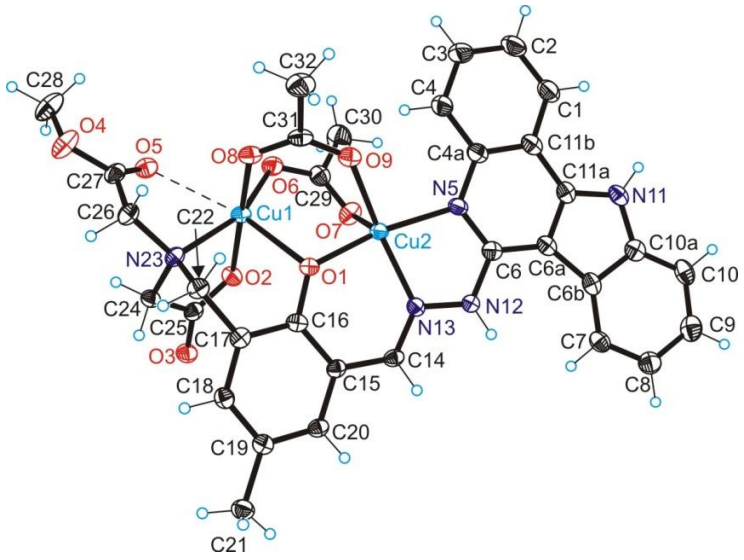

Figure 1. ORTEP view of $[Cu_2(^{MeOOC}\mathbf{L}^{COO})(CH_3COO)_2]$ with thermal ellipsoids drawn at 50% probability level. Selected bond distances (Å) and bond angles (deg): Cu1−O1 2.323(2), Cu1−O2 1.937(2), Cu1−O6 1.946(2), Cu1−O8 1.936(2), Cu1−N23 2.093(3), Cu1···O5 2.946(2), Cu2−O1 1.913(2), Cu2−O7 2.194(2), Cu2−O9 2.002(2), Cu2−N5 2.038(3), Zn2−N13 1.956(3), Cu1−O1−Cu2 101.47(10).

The Zn1–O1 bond distance is only slightly longer than Zn2–O1 as also observed in other complexes with nonsymmetrical dinucleating ligands with a di-μ-acetato-μ-phenolato-dizinc(II) core.[40] The Zn1–O6 bond distance is only slightly longer than Zn2–O7, while

the difference between Zn1–O8 and the shorter bond Zn2–O9 is more pronounced (see caption to Figure 2). The interaction between Zn1 and O5 of the dangling methyl ester group is markedly stronger than comparable interaction in **1**. The Zn1···Zn2 distance in the complex is at 3.2154(7) Å, which is similar with Zn···Zn distance of 3.29(1) Å[40a] in dizinc(II) complex with a nonsymmetrical hybrid ligand.

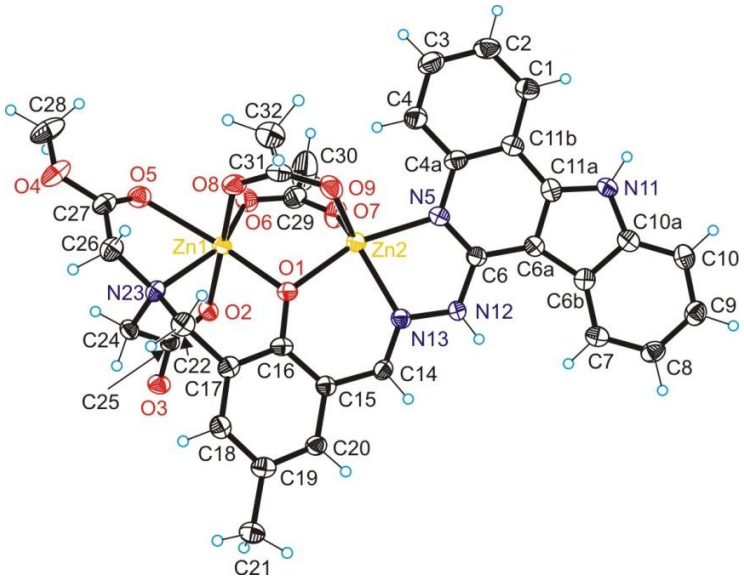

Figure 2. ORTEP view of $[Zn_2(^{MeOOC}L^{COO})(CH_3COO)_2]$ with thermal ellipsoids drawn at 50% probability level. Selected bond distances (Å) and bond angles (deg): Zn1−O1 2.057(3), Zn1−O2 2.105(3), Zn1−O6 2.004(3), Zn1−O8 2.079(3), Zn1−N23 2.149(4), Zn1−O5 2.322(3), Zn2−O1 2.027(3), Zn2−O7 1.991(3), Zn2−O9 1.993(3), Zn2−N5 2.087(4), Zn2−N13 2.097(4), Zn1−O1−Zn2 103.86(14).

Magnetic properties. The magnetic behavior of a polycrystalline sample of **1**·3CH_3OH in the temperature range 2–300 K in a field of 0.1 T is shown in Figure 3**.** The value of

$\chi_M T$ is 0.952 cm^3 K mol^{-1} at 300 K. This value is slightly higher than the expected $\chi_M T$ value (0.750 cm^3 K mol^{-1}) for two noninteracting copper(II) ions (d^9, $g = 2.0$, $S = ½$). The value of $\chi_M T$ continuously increases with decreasing temperature and reaches a value of 1.174 cm^3 K mol^{-1} at 3 K. This behavior suggests the presence of ferromagnetic interactions in **1**·3CH_3OH. According to X-ray diffraction data complex **1**·3CH_3OH has a dinuclear structure, in which the two copper(II) ions are connected by a phenolate oxygen atom and two bidentate briging acetate groups (Figure 1). Therefore, the magnetic behavior can be analysed by using the classical spin Hamiltonian:[28,29,41]

$$H = -2JS_1S_2$$

where J is the exchange coupling constant and $S_1 = S_2 = ½$.

In this case, the Van Vleck equation leads to the following analytical expression:

$$\chi_d = \frac{2Ng_{Cu}^2\beta^2}{Tk_B} \times \frac{1}{3 + e^{-2J/k_BT}}$$

The fitting procedure results in an excellent agreement between the experimental data and the calculated curve (R= 1.4×10^{-6}; Figure 3). The parameters extracted from the fit are J = 3.49(3) cm^{-1}, g = 2.24(1), and zJ = –0.08(1) cm^{-1} and correspond to ferromagnetic interaction between copper(II) ions. The temperature independent paramagnetism (*TIP*) and impurity contribution (ρ) take values close to zero and, both were fixed at zero in the final fit. The presence of ferromagnetic interaction was confirmed by magnetization measurements at low temperature (see inset picture in Figure 3). The fitting of magnetization vs. field by using the Brillouin function indicates the presence of spin ground state S = 1 (g = 2.203(2)) in **1**·3CH_3OH, which is consistent with the results obtained from the analysis of the temperature dependence of magnetic susceptibility.

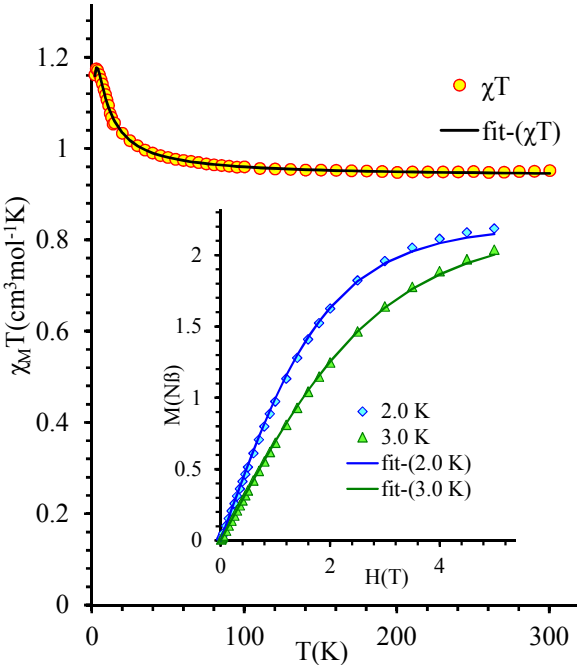

Figure 3. The plots of $\chi_M T$ vs T and magnetization vs. H (inset) at 2 and 3K for **1**·3CH_3OH. The solid lines correspond to the best fit with parameters quoted in the text.

The nature of magnetic interaction in dinuclear copper(II) complexes has been extensively studied from both theoretical and experimental points of view.[42,43,44,45,46,47,48,49,50] The magnetic interaction in **1**·3CH_3OH occurs via three bridges: two μ_2-η^1:η^1 acetato ligands and one bridging phenolate.

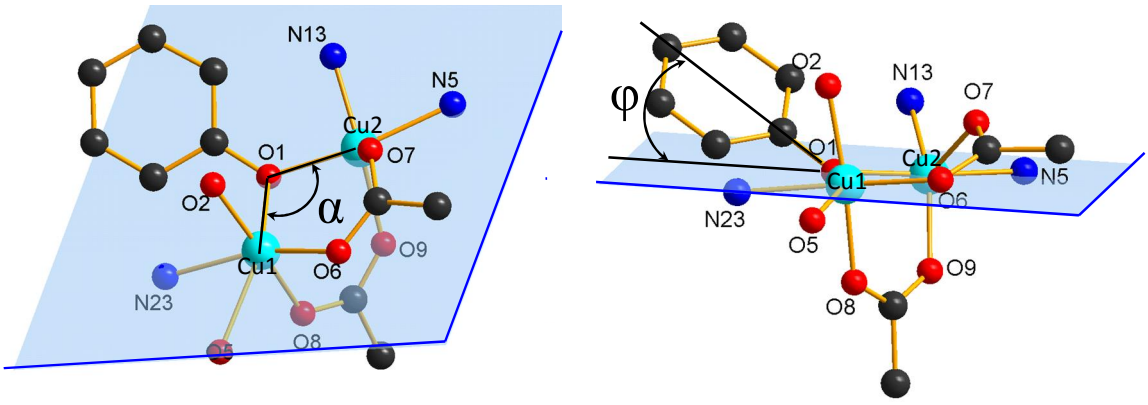

Figure 4. The coordination core in **1**·3CH_3OH showing the angles α and φ.

According to the literature[46] the acetate bridges mediate the antiferromagnetic interactions, while the phenolate bridge in dinuclear copper(II) complexes can promote both antiferromagnetic, as well as ferromagnetic interactions. The character of magnetic interaction depends on geometrical features, and, especially on the Cu–O–Cu angle α, out-of-plane deviation angle φ (see Figure S4) and the torsion angle Cu–O–Cu–O. For α angles <99^o and φ angles >30^o, a strong ferromagnetic interaction can be expected.[46] In the case of **1**·3CH_3OH with α = 101.47 ^{o} and φ = 30.04^o, the presence of a weak ferromagnetic interaction (J = 3.49 cm^{-1}) is justified. We can conclude that due to the out-of-plane deviation of the phenol group relative to Cu–O–Cu plane the resulting magnetic interaction between the triple bridged Cu(II) ions is weekly ferromagnetic. Comparable weekly ferromagnetic interactions were reported for other dinuclear copper(II) dinuclear complexes with two[49,51] or three different bridges.[50,52,53,54,55,56]

Complex Formation Studies. To elucidate whether the two binding sites in ^{EtOOC}**HL**^{COOEt} show different affinities to copper(II), complex formation was studied for **1** via UV–vis titrations of the ligand ^{EtOOC}**HL**^{COOEt} at two different concentrations with copper(II) acetate hydrate in methanol at room temperature (Figures 4 and 5).

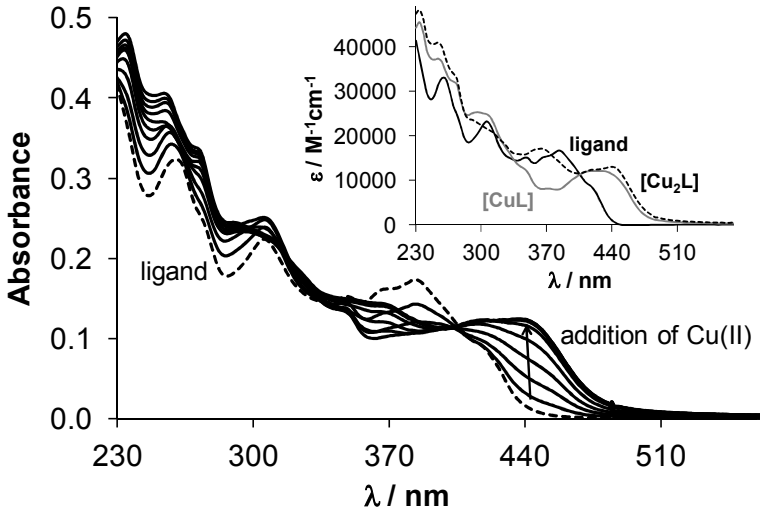

Figure 4. UV–vis absorbance spectrum of the ligand ^{EtOOC}**HL**^{COOEt} (dashed trace) and its changes by the addition of copper(II) acetate monohydrate (solid traces) in methanol (c_L = 10 μM; c_{Cu} = 0 – 22.5 μM; T = 298 K; l = 1 cm). Inset shows the calculated molar absorption spectra of the copper(II) complexes.

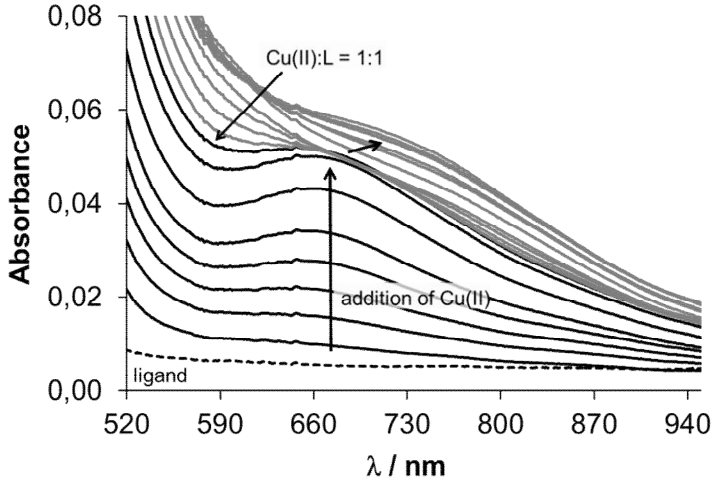

Figure 5. UV–vis absorbance spectrum of the ligand ^{EtOOC}**HL**^{COOEt} (dashed trace) and its changes by the addition of copper(II) (solid traces) in methanol (c_L = 250 μM; c_{Cu} = 0 – 562.5 μM; T = 298 K; l = 1 cm).

The development of a broad charge-transfer band at ca. 440 nm was observed upon addition of up to ~1.5 molar equivalents of copper(II). Then a small shift of the λ_{max} occurred (Figure 4). Characteristic spectral changes have also been registered in the range of the d-d transitions (Figure 5). A wide band with λ_{max} at 664 nm overlapped partly with the charge-transfer band was seen upon addition of copper(II). This absorption band is slightly red-shifted upon addition of more than 1 equiv of copper(II). Based on the spectral changes in the wavelength range 230 – 520 nm (Figure 5) overall stability constants have been calculated for the mono- [CuL] ($\log\beta$ = 7.17 ± 0.08) and dinuclear [Cu_2L] species ($\log\beta$ = 13.13 ± 0.24; $\log K$ = 5.96). The molar absorbance spectra of the ligand, [CuL] and [Cu_2L] complexes were also calculated (Figure 4). The goodness-of-fit between measured and calculated absorbance values is shown in Figure 6. Stability constants obtained by using the changes of the d-d transition bands were in a good agreement with those obtained by monitoring the charge-transfer band within 0.2 log unit. The stepwise formation constant of the [Cu_2L] species is merely ~1 log unit lower than that of the [CuL] showing the overlapping binding of the metal ions. Therefore it can be concluded that both binding sites in ligand $^{EtOOC}\mathbf{HL}^{COOEt}$ coordinate with a similar affinity and no preference for either one can be perceived.

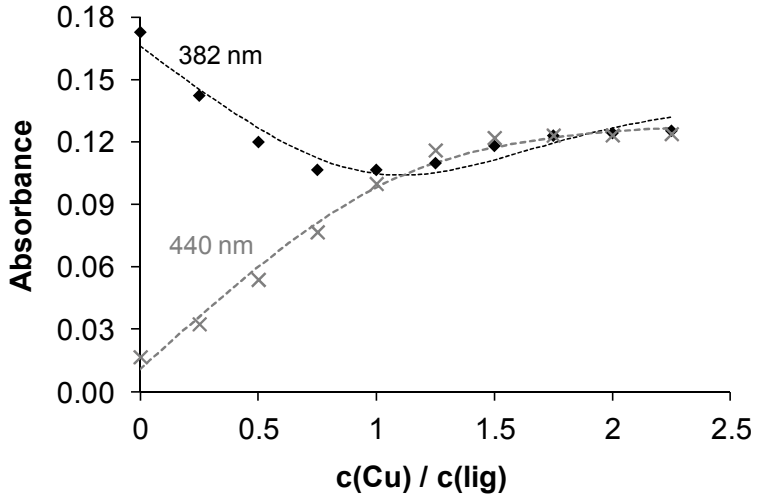

Figure 6. The measured and calculated (dashed lines) absorbance values at 382 nm (♦) and 440 nm (×) at various $^{\mathbf{EtOOC}}\mathbf{HL}^{\mathbf{COOEt}}$-to-copper(II) ratios ($c_L$ = 10 μM; c_{Cu} = 0 – 22.5 μM; T = 298 K; l = 1 cm, methanol).

ESI-MS Studies. The stability of complexes **1** and **2** in aqueous solution and their reactivity towards small biomolecules was studied by ESI mass spectrometry. Both complexes display a very similar aqueous solution behavior, which is characterized by ester hydrolysis of the ligand and partial metal release over time. Products of ester hydrolysis are detected directly after dissolving the compounds in buffer and the ester is quantitatively hydrolyzed within 24 h. The major thermodynamic products after 24 h correspond to ions $[M_2(L–CH_3)(OH) – H^+]^-$ and $[M(L–CH_3) – H^+]^-$, where M = Cu or Zn and L = $^{MeOOC}L^{COO}$ detected in the negative ion mode (Figure 7). The latter mass signal suggests that release of specifically one metal can occur from both **1** and **2**. Interestingly, these signals are detected at 95% and 38% intensities relative to $[M_2(L–CH_3)(OH) – H^+]^-$ for **1** and **2**, respectively, *i.e.* the Cu-complex **1** releases one metal-equivalent to a greater extent. Therefore, complex **2** appears to be slightly more stable in aqueous solution.

Additionally, **2** does not ionize in the positive ion mode, suggesting stable bonds between Zn ions and the acetate ligands (Figure S2). Note that acetato-complexes were not detected at all in the mass spectra of **1** or **2**. Furthermore, the isotopic distributions of the mass signals of **2** indicate the formation of redox couples (Figure S3). Both complexes were exposed to mixtures containing equimolar amounts of His, Asp, Glu and GTP. The complexes did not react with any of the biological nucleophiles and similar mass spectra were observed compared to the solutions containing only the respective metal. Addition of 4 equiv of Asc to the amino acids resulted in the transient formation of Glu- and Asc-adducts with **1** in a small amount, however, they were only detected immediately after mixing (Figure 7, C) and were absent for **2**. Free ascorbate was consumed within 1 h, but had no impact on the overall reactivity of the complexes. An interesting feature of both compounds is their ability to release a metal ion in a pH-dependent manner (Figure S4). The samples incubated for 24 h displayed only partial metal-release. Lowering the pH of this incubation solution with formic acid resulted in the immediate and quantitative release of one metal from both dimetallic complexes. It is suggested that the carboxylates are prone to protonation under these conditions, leading to the release of the octahedral coordinated metal.

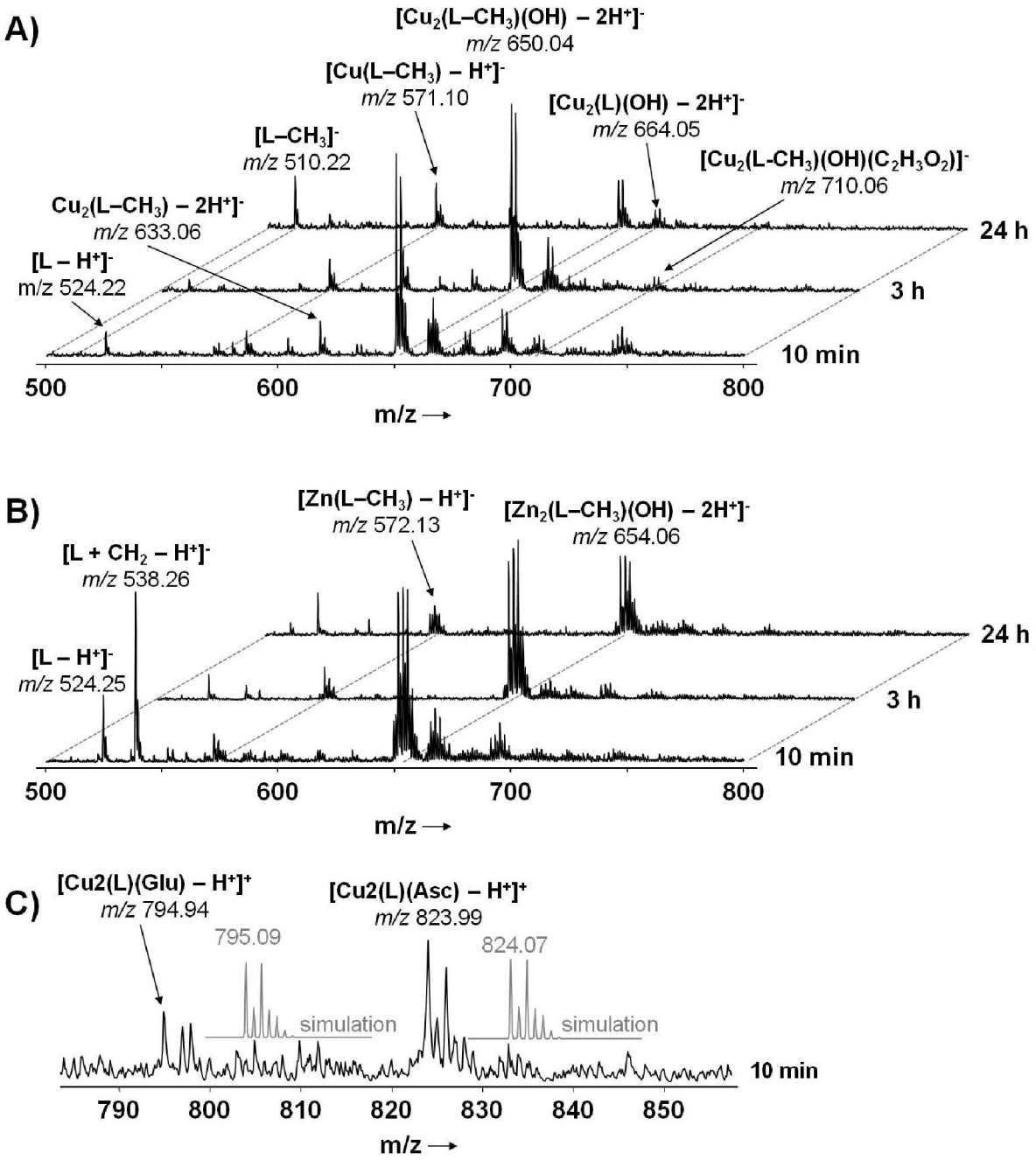

Figure 7. The ESI mass spectra in the negative ion mode are shown for **1** (A) and **2** (B). The istotopic distributions of the most abundant mass signals are shown on the right. The isotopic pattern of $[Zn_2(L–CH_3)(OH) – 2H^+]^+$ seems to involve redox couples. Simulations are shown in grey. The Glu- and Asc-adducts of **1** are displayed in (C) directly after mixing.

Fluorescence Properties. Fluorescence spectra of $^{EtOOC}HL^{COOEt}$ and **2** were recorded in HEPES buffered solutions (20 mM; pH = 7.4) with a 1% v/v content of DMSO (Figure 8). Fluorescence excitation spectra (λ_{em} = 470 nm) were measured in the range between 260 and 460 nm and emission spectra (λ_{ex} = 395 nm) in the range from 410 to 710 nm. The emission maximum of the ligand was observed at 532 nm. Coordination to zinc(II) led to a blue-shift of the emission band by 54 nm, with the maximum at 466 nm in the spectra of **2**. $^{EtOOC}HL^{COOEt}$ was found fluorogenic, as excitation and emission spectra strongly increased in intensity upon binding to zinc(II).

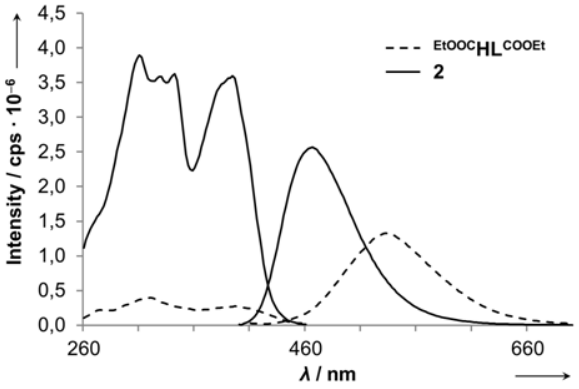

Figure 8: Fluorescence excitation (λ_{em} = 470 nm) and emission (λ_{ex} = 395 nm) spectra of 10 μM solutions of $^{EtOOC}HL^{COOEt}$ (dashed traces) and **2** (solid traces) at physiological pH (20 mM HEPES buffer, 1% v/v DMSO).

Cytotoxicity in Cancer Cells. The cytotoxicity of $^{EtOOC}HL^{COOEt}$, **1** and **2** was determined by the MTT assay in three human cancer cell lines, namely, A549 (non-small cell lung carcinoma), CH1 (ovarian carcinoma) and SW480 (colon adenocarcinoma), all yielding IC_{50} values in the micromolar concentration range (Table 2**)**.

Table 2. Cytotoxicity of ligand ^{EtOOC}**HL**^{COOEt}, complexes **1** and **2** in three human cancer cell lines.

	IC_{50} (μM), 96 h[a]		
	^{EtOOC}**HL**^{COOEt}	**1**	**2**
A549	28 ± 2	30 ± 4	12 ± 1
CH1	2.2 ± 0.3	6.6 ± 1.3	1.6 ± 0.4
SW480	16 ± 2	22 ± 2	7.8 ± 0.3

[a]50% inhibitory concentrations (means ± standard deviations from at least three independent experiments), as obtained by the MTT assay using exposure times of 96 h.

CH1 was the most sensitive cell line to all tested compounds, whereas A549, a more chemoresistant cell line, was the least sensitive one. In CH1 cells the compounds were up to 12 times more potent than in A549 cells. Whereas complexation with copper(II) has either little effect on cytotoxicity (A549, SW480 cells) or yields 3-fold decreased potency (CH1 cells), complexation with zinc(II) results in about twofold enhancement of cytotoxicity, in all three cell lines, compared to the metal free ligand ^{EtOOC}**HL**^{COOEt}. In comparison to the dicopper(II) complex **1**, the dizinc(II) complex **2** is up to three times more active in SW480 and four times more active in CH1 cells (see also Figure 7). Based on these observations, it can be concluded that complexation to zinc(II) results in higher cytoxicity and better solubility in biocompatible media compared to both the metal-free ligand and copper(II) complex **1**.

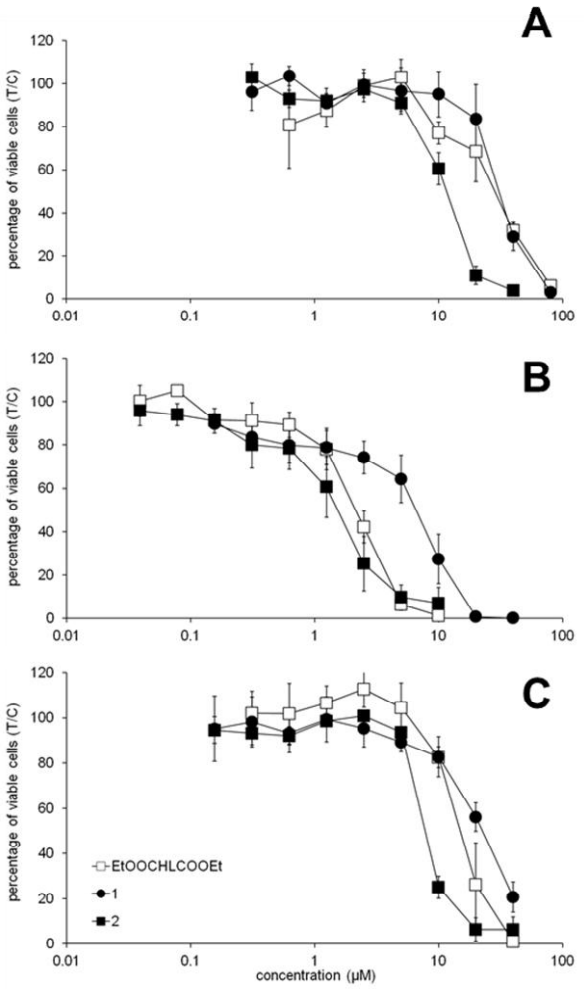

Figure 7. Concentration-effect curves of $^{EtOOC}HL^{COOEt}$, complexes **1** and **2**, in the human cancer cell lines A549 (A), CH1 (B) and SW480 (C), determined by the MTT assay using continuous exposure for 96 h.

Fluorescence Microscopy. Based on the fluorescence properties of $^{EtOOC}\mathbf{HL}^{COOEt}$ and dizinc(II) complex **2**, their subcellular localization was studied by fluorescence microscopy in human cancer cells including their co-localization with organelle-specific dyes. For visualization of the compounds in live SW480, A549 and CH1 cells the U-MG2 (Olympus Japan) filter was used, while the co-staining dyes were recorded using the U-MGU2 (Olympus Japan) filter. The compounds do not show interference in the U-MGU2 channel and auto-fluorescence of the cells was not observed with the used filters. The microscopic images of $^{EtOOC}\mathbf{HL}^{COOEt}$ and **2**, as shown in Figure 8, revealed localization of the compounds in cytoplasmic structures. The highest accumulation of the compounds matches with both the ER-Tracker Red and Lyso-Tracker Red staining, suggesting that the endoplasmic reticulum as well as the lysosomes can be potential targets of these compounds or that lysosomes are involved in sequestration and/or detoxification of the compounds.

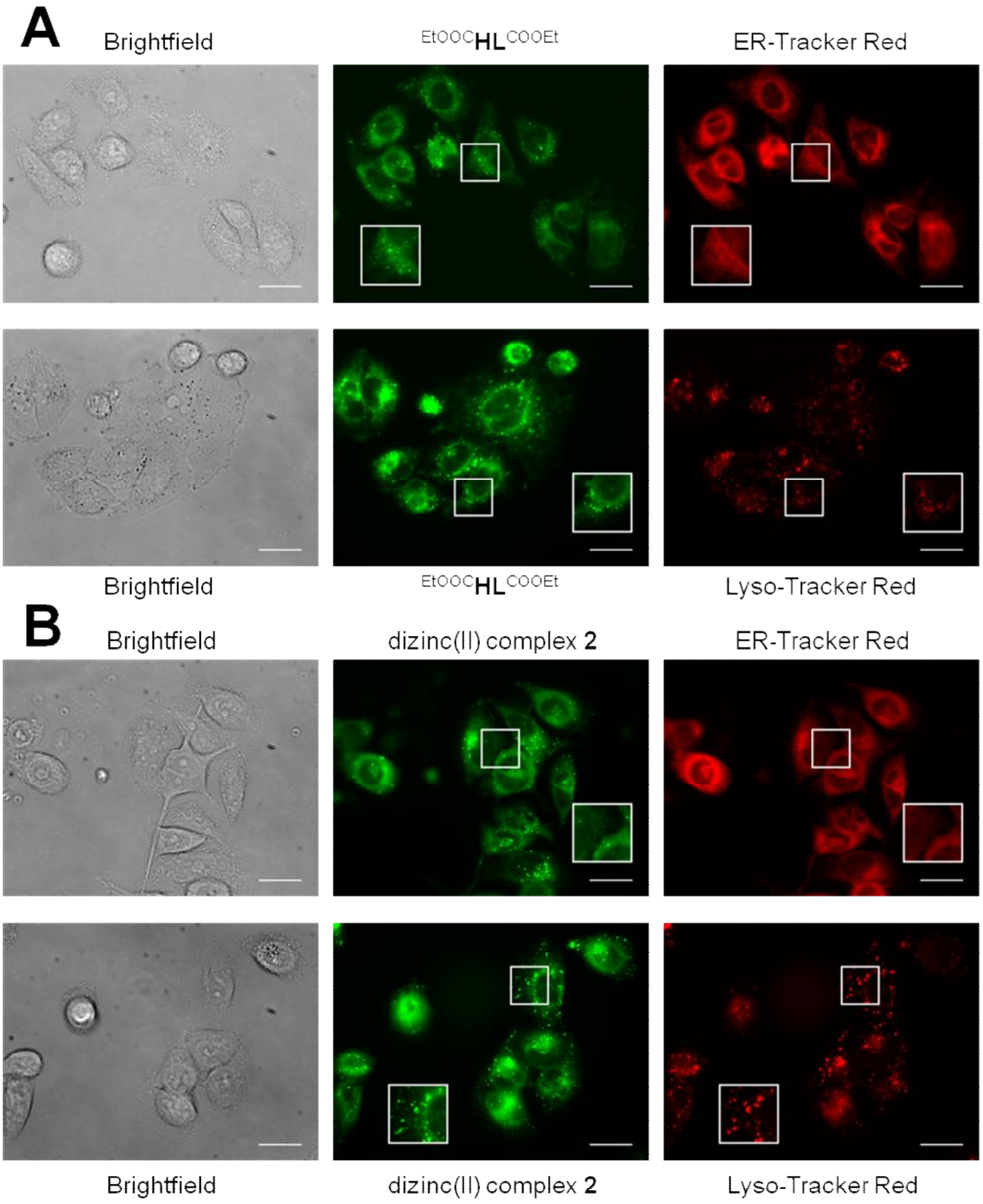
A
Brightfield
EtOOCHLCOOEt
ER-Tracker Red
Brightfield
EtOOCHLCOOEt
Lyso-Tracker Red
B
Brightfield
dizinc(II) complex 2
ER-Tracker Red
Brightfield
dizinc(II) complex 2
Lyso-Tracker Red

Figure 8. Fluorescence microscopy images of live SW480 cells. Cells were co-stained with 10 μM of $^{EtOOC}\mathbf{HL}^{COOEt}$ (A) or 5 μM of **2** (B) and ER-Tracker Red (500 nM) and Lyso-Tracker Red (1 μM), respectively. Magnification of areas marked by squares, are shown as insets. Scale bars are 20 μm.

Conclusion

Condensation of 6-hydrazinyl-11*H*-indolo[3,2-*c*]quinoline with diethyl-2,2′-((3-formyl-2-hydroxy-5-methylbenzyl)azanediyl)diacetate afforded a new nonsymmetric dinucleating ligand $^{EtOOC}\mathbf{HL}^{COOEt}$ with increased aqueous solubility and fluorescence properties. In the presence of 2 equiv $Cu(CH_3COO)_2 \cdot H_2O$ and $Zn(CH_3COO)_2 \cdot 2H_2O$ in methanol complexes **1** and **2** are formed. Complexation reaction in both cases is accompanied by hydrolysis of one ethyl ester group and transesterification of another ethyl ester function with formation of $^{MeOOC}\mathbf{HL}^{COOH}$. Dinuclear structure in **1**·$3CH_3OH$ and **2**·$3CH_3OH$ is supported by three bridges: two acetato ligands and one phenolate bridge from nonsymmetric $^{MeOOC}\mathbf{HL}^{COOH}$ ligand. The temperature dependence and field dependence magnetic measurements for **1**·$3CH_3OH$ indicate a weak ferromagnetic interaction (J = 3.49 cm^{-1}) between copper(II) ions. All three compounds show respectable antiproliferative activity in human cancer cell lines (A549, CH1, SW480) with IC_{50} values in the micromolar concentration range. Localization of $^{EtOOC}\mathbf{HL}^{COOEt}$ and **2** in cytoplasmic structures has been found by fluorescence microscopy, suggesting that the endoplasmic reticulum as well as the lysosomes can be potential targets of these compounds.

Supporting Information

Further details are given in Figures S1-S4 and Table S1, and crystallographic data is given in CIF format.

Corresponding Author

*E-mail: vladimir.arion@univie.ac.at (V. B. A.).

Notes

The authors declare no competing financial interest.

Acknowledgments. We thank Alexander Roller for collection of X-ray data for **1** and **2**. This work was financially supported by the University of Vienna within the doctoral program, "Initiativkolleg Functional Molecules" (IK I041-N) and the Austrian Science Fund (Project no P22339-N19).

References

(1) Colditz, G. A; Sellers, T. A; Trapido, E. *Nat. Rev. Cancer* **2006**, *6*, 75–83.

(2) Umar, A.; Dunn, B. K.; Greenwald, P. *Nat. Rev. Cancer* **2012**, *12*, 835–848.

(3) Kim, M.-S. *Biomol. Ther.* **2011**, *19*, 371–389.

(4) Jakupec, M. A.; Galanski, M.; Arion, V. B.; Hartinger, C. G.; Keppler, B. K. *Dalton Trans.* **2008**, 183–194.

(5) Hartinger, C. G.; Dyson, P. J. *Chem. Soc. Rev.* **2009**, *38*, 391–401.

(6) Jungwirth, U.; Kowol, C. R.; Keppler, B. K.; Hartinger, C. G.; Berger, W.; Heffeter, P. *Antioxidants Redox Signaling* **2011**, *15*, 1085–1127.

(7) Gasser, G.; Metzler-Nolte, N. *Curr. Opin. Chem. Biol.* **2012**, *16*, 84–91.

(8) Zaharevitz, D. W.; Gussio, R.; Leost, M.; Senderowicz, A. M.; Lahusen, T.; Kunick, C.; Meijer, L.; Sausville, E. A. **1999**, *59*, 2566–2569.

(9) Kelland, L. R. *Expert Opin. Investig. Drugs,* **2000**, *9*, 2903–2911.

(10) Tolle, N.; Kunick, C. *Curr. Top. Med. Chem.* **2011**, *11*, 1320–1332.

(11) Primik, M. F.; Mühlgassner, G.; Jakupec, M. A.; Zava, O.; Dyson, P. J.; Arion, V. B.; Keppler, B. K. *Inorg. Chem.* **2010**, *49*, 302–311.

(12) Dobrov, A.; Arion, V. B.; Kandler, N.; Ginzinger, W.; Jakupec, M. A.; Rufińska, A.; Graf von Keyserlingk, N.; Galanski, M.; Kowol, C.; Keppler, B. K. *Inorg. Chem.* **2006**, *45*, 1945–1950.

(13) Ginzinger, W.; Arion, V. B.; Giester, G.; Galanski, M.; Keppler, B. K. *Centr. Eur. J. Chem.* **2008**, *6*, 340–346.

(14) Schmid, W. F.; John, R. O.; Arion, V. B.; Jakupec, M. A.; Keppler, B. K. *Organometallics* **2007**, *26*, 6643–6652.

(15) Arion, V. B.; Dobrov, A.; Göschl, S.; Jakupec, M. A.; Keppler, B. K.; Rapta, P. *Chem. Commun.* **2012**, *48*, 8559–8561.

(16) Lavrado, J.; Moreira, R.; Paulo, A. *Curr. Med. Chem*. **2010**, *17*, 2348–2370.

(17) Filak, L. K.; Mühlgassner, G.; Jakupec, M. A.; Heffeter, P.; Berger, W.; Arion, V. B.; Keppler, B. K. *J. Biol. Inorg. Chem.* **2010**, *15*, 903–918.

(18) Filak, L. K.; Mühlgassner, G.; Bacher, F.; Roller, A.; Galanski, M.; Jakupec, M. A.; Keppler, B. K.; Arion, V. B. *Organometallics* **2011**, *30*, 273–283.

(19) Primik, M. F.; Göschl, S.; Jakupec, M. A; Roller, A.; Keppler, B. K.; Arion, V. B. *Inorg. Chem.* **2010**, *49*, 11084-11095.

(20) Filak, L. K.; Göschl, S.; Hackl, S.; Jakupec, M. A.; Arion, V. B. *Inorg. Chim. Acta* **2012**, *393*, 252–260.

(21) Filak, L. K.; Göschl, S.; Heffeter, P.; Ghannadzadeh Samper, K.; Egger, A. E.; Jakupec, M. A; Keppler, B. K.; Berger, W.; Arion, V. B. *Organometallics* **2013**, *32*, 903–914.

(22) Huisman, M.; Koval, I. a.; Gamez, P.; Reedijk, J. *Inorg. Chim. Acta* **2006**, *359*, 1786–1794.

(23) Wang, Q.; Wilson, C.; Blake, A. J.; Collinson, S. R.; Tasker, P. A.; Schröder, M. *Tetrahedron Lett.* **2006**, *47*, 8983–8987.

(24) SAINT-*Plus*, version 7.06a and APEX2; Bruker-Nonius AXS Inc.: Madison, WI, 2004.

(25) Sheldrick, G. M., *Acta Crystallogr.* **2008**, *A46*, 112–122.

(26) Burnett, M. N.; Johnson, G. K. *ORTEPIII*. Report ORNL-6895; OAK Ridge National Laboratory: Oak Ridge, TN, 1996.

(27) Pascal, P. *Ann. Chim. Phys.* **1910**, *19*, 5–70.

(28) Kahn, O. *Molecular Magnetism,* VCH Publishers, Inc.: New York, Weinheim, Cambridge, 1993.

(29) O'Connor, C. J. *Prog. Inorg. Chem.* **1982**, *29*, 203–.

(30) Myers, B. E.; Berger, L.; Friedber, S. A. *J. Appl. Phys.* **1969**, *40*, 1149–.

(31) Zékány, L.; Nagypál, I. in: Computational Methods for the Determination of Stability Constants (Ed.: D. L. Leggett), Plenum Press, New York, 1985, p. 291–353.

(32) Hatfield, J. M.; Wierdl, M.; Wadkins, R. M.; Potter, P. M. *Exp. Opin. Drug Metabol. Toxicol.* **2008**, *4*, 1153–1165.

(33) Milunovic, M. N. M.; Enyedy, É. A; Nagy, N. V.; Kiss, T.; Trondl, R.; Jakupec, M. A; Keppler, B. K.; Krachler, R.; Novitchi, G.; Arion, V. B. *Inorg. Chem.* **2012**, *51*, 9309–9321.

(34) Bußkamp, H.; Deacon, G. B.; Hilder, M.; Junk, P. C.; Kynast, U. H.; Lee, W. W.; Turner, D. R. *CrystEngComm* **2007**, *9*, 394–411.

(35) Addison, A. W.; Rao, T. N.; Reedijk, J.; van Rijn, J.; Verschoor, C. G. *J. Chem. Soc. Dalton Trans.* **1984**, 1349–1356.

(36) Lubben, M.; Hage, R.; Meetsma, A.; Bÿma, K.; Feringa, B. L. *Inorg. Chem.* **1995**, *34*, 2217–2224.

(37) Adams, H.; Candeland, G.; Crane, J. D.; Fenton, D. E.; Smith, A. J. *Chem. Commun.* **1990**, 93–95.

(38) Nishida, Y.; Tokii, T.; Mory, Y. *J. Chem. Soc. Chem. Commun.* **1988**, 675-;

(39) Bertoncello, K.; Fallon, G. D.; Hodgkin, J. H.; Murray, K. S. *Inorg. Chem.* **1988**, *27*, 4750–4758.

(40) (a) Abe, K.; Izumi, J.; Ohba, M.; Yokoyama, T.; Okawa, H. *Bull. Chem. Soc. Jpn.* **2001**, *74*, 85–95; (b) Adams, H.; Cummings, L. R.; Fenton, D. E.; McHugh, P. E. *Inorg. Chem. Commun.* **2003**, *6*, 19–22.

(41) Bleaney, B.; Bowers, K. D. *Proc. Royal Soc. London Ser.-Math. Phys. Sci.* **1952,** *214*, 451–465.

(42) Melník, M., *Coord. Chem. Rev.* **1982**, *42*, 259–293.

(43) Onofrio, N.; Mouesca, J.-M., *J. Phys. Chem. A* **2010,** *114*, 6149–6156.

(44) Ruiz, E.; Alemany, P.; Alvarez, S.; Cano, J. *Inorg. Chem.* **1997,** *36*, 3683–3688.

(45) Blanchet-Boiteux, C.; Mouesca, J.-M., *Theor. Chem. Acc.* **2000,** *104*, 257–264.

(46) Venegas-Yazigi, D.; Aravena, D.; Spodine, E.; Ruiz, E.; Alvarez, S. *Coord. Chem. Rev.* **2010,** *254*, 2086–2095.

(47) Kato, M.; Muto, Y. *Coord. Chem. Rev.* **1988**, *92*, 45–83.

(48) Kahn, O. *Comm. Inorg. Chem.* **1984**, *3*, 105–132.

(49) Lopez, C.; Costa, R.; Illas, F.; De Graaf, C.; Turnbull, M. M.; Landee, C. P.; Espinosa, E.; Mata, I.; Molins, E. *Dalton Trans.* **2005,** 2322–2330.

(50) Costa, R.; Moreira, I. R. D. P. R.; Youngme, S.; Siriwong, K.; Wannarit, N.; Illas, F. *Inorg. Chem.* **2010,** *49*, 285–294.

(51) Fondo, M.; García-Deibe, Ana M.; Sanmartín, J.; Bermejo, Manuel R.; Lezama, L.; Rojo, T. *Eur. J. Inorg. Chem.* **2003,** 3703–3706.

(52) Christou, G.; Perlepes, S. P.; Libby, E.; Folting, K.; Huffman, J. C.; Webb, R. J.; Hendrickson, D. N. *Inorg. Chem.* **1990,** *29*, 3657–3666.

(53) Youngme, S.; Phatchimkun, J.; Wannarit, N.; Chaichit, N.; Meejoo, S.; van Albada, G. A.; Reedijk, J. *Polyhedron* **2008,** *27*, 304–318.

(54) Chailuecha, C.; Youngme, S.; Pakawatchai, C.; Chaichit, N.; van Albada, G. A.; Reedijk, J. *Inorg. Chim. Acta* **2006**, *359*, 4168–4178.

(55) Youngme, S.; Chailuecha, C.; van Albada, G. A.; Pakawatchai, C.; Chaichit, N.; Reedijk, J. *Inorg. Chim. Acta* **2004,** *357*, 2532–2542.

(56) Youngme, S.; Chailuecha, C.; van Albada, G. A.; Pakawatchai, C.; Chaichit, N.; Reedijk, J. *Inorg. Chim. Acta* **2005,** *358*, 1068–1078.

Table of Contents